Real-time highlight removal using intensity ratio

Hui-Liang Shen* and Zhi-Huan Zheng

Department of Information Science and Electronic Engineering, Zhejiang University, Hangzhou 310027, China

*Corresponding author: shenhl@zju.edu.cn

Received 28 March 2013; revised 23 May 2013; accepted 24 May 2013;
posted 24 May 2013 (Doc. ID 187931); published 24 June 2013

In this paper, we propose an efficient method to separate the diffuse and specular reflection components from a single image. The method is built on the observation that, for diffuse pixels, the intensity ratios between the maximum values and range values (maximums minus minimums) are independent of surface geometry. The specular fractions of the image pixels can then be computed by using the intensity ratio. For textured surfaces, image pixels are classified into clusters by constructing a pseudo-chromaticity space, and the intensity ratio of each cluster is robustly estimated. Unlike existing techniques, the proposed method works in a pixel-wise manner, without specular pixel identification and any local interaction. Experimental results show that the proposed method runs 4× faster than the state of the art and produces improved accuracy in specular highlight removal.

OCIS codes: (150.1135) Algorithms; (120.5700) Reflection; (330.1690) Color.
http://dx.doi.org/10.1364/AO.52.004483

1. Introduction

It is a common assumption in the computer vision community that scene surfaces are of pure diffuse reflection. However, for a wide variety of inhomogeneous materials in the real world, the reflection includes both diffuse and specular components. Hence it is quite possible that the algorithms based on an ideal Lambertian assumption will produce erroneous outputs. Because of its important role in low-level computer vision, in recent years specular reflection has attracted much attention in fields such as edge detection [1], color constancy [2,3], stereo correspondence [4], and photometric stereo [5,6].

Diffuse and specular reflections are formed by different physical interactions between light and object surfaces. When a light ray strikes the surface of inhomogeneous matter, part of it is immediately reflected at the interface between the object surface and the air and is referred as specular reflection or highlight. In addition, part of the light will penetrate the interface and enter the object, where it keeps striking the colorants and is scattered by the colorants. Partially scattered light arrives back at the object surface and re-enters the air, and is referred to as diffuse reflection. According to the neutral interface reflection model [7], the color of the specular reflection is identical to that of the illumination, while the color of the diffuse reflection is the intrinsic characteristic of the object.

For practical applications in the computer vision fields, the specular reflection component needs to be removed from a single image. When functioning as a preprocessing step, it is preferred that the algorithm run in real time. In this paper we propose a specular reflection separation method that is simple yet efficient in implementation. It is built on the observation that the intensity ratios of diffuse pixels are independent on surface geometry and are lower than those of specular pixels. Using pixel clustering and intensity ratio sorting, the specular component of each pixel can be determined. The proposed method works in a pixel-wise manner, without specular pixel identification and any local interaction. Experiments are conducted to evaluate the proposed method on real images quantitatively and qualitatively.

1559-128X/13/194483-11$15.00/0

A. Prior Art

Many studies have been conducted to separate specular reflection from either multiple images or a single image [8–20]. The dichromatic reflection model, first introduced by Shafer [21], was widely employed in this work.

Based on the observation that the specular reflection is polarized while the diffuse reflection is not, Nayar *et al.* [14] employed a polarization filter to determine the color of the specular highlight and then separated the diffuse reflection component. However, the additional use of a polarization filter makes the method unsuitable for many practical applications.

A number of studies attempted to separate reflection components by using multiple images. Sato and Ikeuchi [10] separated reflections locally in a temporal-color space, based on the color changes at individual pixels. In multibaseline stereo, Lin *et al.* [15] removed highlights based on the assumption that pixels have specular reflection under some views while containing pure diffuse reflection in other views. In photometric stereo, Barsky and Petrou [22] identified specular pixels according to the intensity distribution and separated the specular component by using the dichromatic reflection model.

In recent years, considerable effort has been devoted to specular reflection separation in a single image. By regarding highlight removal as an interactive inpainting process, Tan *et al.* [16] recovered the diffuse colors of specular pixels under illumination constraints. Klinker *et al.* [9] observed that the diffuse and specular components of uniform color surfaces form a skewed T shape in the color histogram, and they proposed to separate these two components by using convex polygon fitting. Their method will fail on textured surfaces whose histograms are not T shaped. Tan and Ikeuchi [12] demonstrated that, with their introduced specular-free (SF) image, the reflection on heavily textured surfaces could be reliably separated without image segmentation. Their method works in an iterative framework by shifting the chromaticity values of specular pixels toward to those of neighboring pixels having maximum chromaticity values in each iteration. Tan and Ikeuchi [12] further presented reflection separation methods based on noise and chromaticity analysis [11] and reflectance basis functions [13]. Shen *et al.* [18] classified image pixels into diffuse and specular candidates and determined the specular component by solving the dichromatic least-squares system. Mallick *et al.* [17] separated reflection components in image and video by using an illumination-independent color space and partial differential equation.

Most recently, several fast methods for specular component separation have been proposed. Shen and Cai [20] approximated the chromaticity of diffuse reflection by that of a SF image and adjusted the highlight level by enforcing smooth color transition between diffuse and specular regions. Based on the framework of Tan and Ikeuchi [12], Yang *et al.* [19] proposed a method by applying bilateral filtering to the maximum fraction of the original color component, with the aim to propagate the maximum diffuse chromaticity values of diffuse pixels to those of specular ones. Their method is computationally efficient and usually converges after several iterations.

B. Our Contribution

To date, most reflection separation methods employ either iterative frameworks or solve linear (or nonlinear) systems, making them inapplicable in real-time applications. To the best of our knowledge, the only exception is Yang's method [19], which is based on fast bilateral filtering.

In this paper, we propose an efficient and effective method to separate diffuse and specular reflection components in a single image. This method is based on the observation that, for a diffuse pixel, the intensity ratio between maximum value and range value (maximum minus minimum) is independent of surface geometry. Hence, by assuming that a certain proportion of pixels contains only diffuse reflection, the specular components of other pixels can be easily computed by using the estimated intensity ratio of diffuse pixels. This method can be easily extended to textured surfaces, by clustering pixels according to their pseudo-chromaticity values. Unlike previous techniques, the proposed method does not require specular pixel identification and local pixel interaction, and thus is simple in implementation and efficient in computation.

2. Proposed Method

In this section, we first briefly review the dichromatic reflection model and then present the concept of intensity ratio, followed by pixel clustering for a nonuniform and textured object surface. Finally, we outline the implementation of the proposed method.

A. Reflection Model

According to the dichromatic reflection model [21], the RGB color $\mathbf{I}(x) = [I_r(x), I_g(x), I_b(x)]^T$ at pixel x is the linear combination of the diffuse reflection $\mathbf{I}^D(x)$ and specular reflection $\mathbf{I}^S(x)$. Due to their reflective characteristics, these two reflections can be further represented by the diffuse chromaticity $\Lambda = [\Lambda_r, \Lambda_g, \Lambda_b]^T$ and illumination chromaticity $\mathbf{\Gamma} = [\Gamma_r, \Gamma_g, \Gamma_b]^T$, respectively:

$$\mathbf{I}(x) = \mathbf{I}^D(x) + \mathbf{I}^S(x) = m_d(x)\Lambda + m_s(x)\mathbf{\Gamma}, \quad (1)$$

where $m_d(x)$ and $m_s(x)$ are the surface-geometry-related weights for the diffuse and specular reflections, respectively.

It is noted that, for the image pixels, the diffuse chromaticity values Λ are identical for uniform color surfaces, but different for nonuniform or textured

surfaces. The illumination chromaticity $\mathbf{\Gamma}$ can be directly acquired by imaging a white board, or can be otherwise estimated from the image [2,3,23]. In the following, we assume that the RGB colors are normalized with respect to the illumination color such that $\mathbf{\Gamma} = [\Gamma, \Gamma, \Gamma]^T$, with $\Gamma = 1/3$. After normalization, the illumination is of white color.

B. Intensity Ratio

An image usually contains a proportion of pixels with pure diffuse reflection. Based on this, we propose the concept of intensity ratio, which is the ratio between the maximum value and range value (maximum minus minimum) of the diffuse pixel, to remove the specular highlight in the image.

In this subsection, we limit our discussion on uniform color surfaces for clarity of discussion. The concept of intensity ratio will be extended to nonuniform and textured surfaces in the next subsection.

For an uniform color surface, the pixels have the same diffuse chromaticity Λ. We obtain the minimum intensity of pixel x by taking its minimum value of the RGB channels:

$$\begin{aligned} I_{\min}(x) &= \min\{I_r(x), I_g(x), I_b(x)\} \\ &= m_d(x)\Lambda_{\min} + m_s(x)\Gamma, \end{aligned} \tag{2}$$

where $\Lambda_{\min} = \min\{\Lambda_r, \Lambda_g, \Lambda_b\}$. In a similar manner, we obtain the maximum intensity

$$I_{\max}(x) = m_d(x)\Lambda_{\max} + m_s(x)\Gamma, \tag{3}$$

where $\Lambda_{\max} = \max\{\Lambda_r, \Lambda_g, \Lambda_b\}$. Clearly, for pixels with pure diffuse reflection, $I_{\min}(x) = m_d(x)\Lambda_{\min}$ and $I_{\max}(x) = m_d(x)\Lambda_{\max}$.

In Eqs. (2) and (3), the minimum and maximum intensities have the same specular term $m_s(x)\Gamma$. By subtracting the minimum intensity from the maximum one, we obtain the range intensity as

$$I_{\text{ran}}(x) = I_{\max}(x) - I_{\min}(x) = m_d(x)(\Lambda_{\max} - \Lambda_{\min}), \tag{4}$$

which eliminates the specular term $m_s(x)\Gamma$.

We define the intensity ratio between the maximum and range values as

$$Q(x) = \frac{I_{\max}(x)}{I_{\text{ran}}(x)}. \tag{5}$$

For a pixel that does not contain specular reflection, the intensity ratio is

$$Q_d(x) = \frac{\Lambda_{\max}}{\Lambda_{\max} - \Lambda_{\min}}, \tag{6}$$

which is clearly independent of surface geometry. We note that, if $Q(x)$ is defined as the ratio $I_{\min}/I_{\text{ran}}$, the geometry-independent property of $Q_d(x)$ also holds. However, compared with $I_{\max}$, $I_{\min}$ values are more likely to be affected by image noise, and thus we use the intensity ratio defined in Eq. (5). If we denote Q_d as the true value of $\Lambda_{\max}/(\Lambda_{\max} - \Lambda_{\min})$, $Q_d(x)$ usually biases from Q_d due to image noise. In practical computation, the denominator can be replaced by $(\Lambda_{\max} - \Lambda_{\min} + \varepsilon)$, where $\varepsilon \geq 0$ is a small value, so that $Q_d(x)$ remains stable when $\Lambda_{\max} \approx \Lambda_{\min}$.

The intensity ratio of a specular pixel is

$$Q_s(x) = \frac{\Lambda_{\max}}{\Lambda_{\max} - \Lambda_{\min}} + \frac{m_s(x)\Gamma}{m_d(x)(\Lambda_{\max} - \Lambda_{\min})}, \tag{7}$$

which is relevant to both the geometry terms $m_d(x)$ and $m_s(x)$. Similarly, Q_s only applies to chromatic surface colors. It is clear from Eqs. (6) and (7) that, for pixels with identical chromaticity Λ, the intensity ratios of specular pixels are larger than those of diffuse pixels, i.e., $Q_s(x) > Q_d(x)$. Figure 1 shows the distribution of intensity ratios along an image row of a real object surface. It is observed that, for the diffuse pixels located far from the highlight spot, the intensity ratios are low and keep approximately constant. This agrees well with the theoretic analysis above. For the visually diffuse pixels near the highlight spot, the intensity ratios still depend on surface geometry, as these pixels actually contain a small portion of specular component. It seems that, in case of widespread specular reflection, the determination of intensity ratios of diffuse pixels is not easy. Nevertheless, we can still distinguish the less specular pixels from others by using their intensity ratio, as will be shown in the following.

Our objective is to estimate the true intensity ratio Q_d of diffuse pixels, based on which the specular components of other pixels can be consequently determined. However, it is a nontrivial problem to classify diffuse and specular pixels accurately [12,24]. Fortunately, we can avoid this problem based on the observation that $Q_d(x) < Q_s(x)$ for pixels with identical diffuse chromaticity values. In this regard, we sort the pixels in a nondescending order with respect to their intensity ratios $Q(x)$. By assuming that the proportion of diffuse pixels is less than a percentile threshold T_P, we locate the pixel $\hat{x}$ whose rank satisfies $\text{rank}(Q(\hat{x})) = \lceil T_P L \rceil$, where the operator $\lceil \cdot \rceil$ rounds the variable to the nearest integer

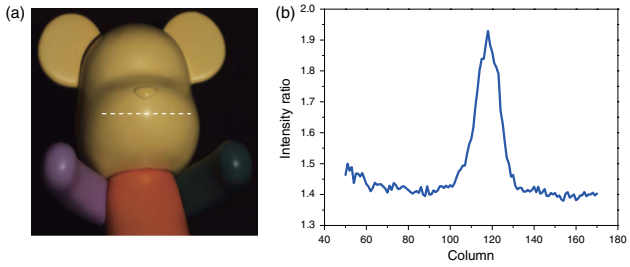

Fig. 1. Illustration of intensity ratio on a real object. (a) Object image, (b) intensity ratios along the marked image row.

and L denotes the number of pixels. Then Q_d is estimated as

$$\hat{Q}_d = Q(\hat{x}). \tag{8}$$

As a special case, when $T_P = 50\%$, the estimate of Q_d becomes

$$\hat{Q}_d = \underset{x\in\Omega}{\text{median}}\{Q(x)\}, \tag{9}$$

where Ω denotes the pixel set.

We note that, for a region with widespread specular component, the intensity ratios of the majority of pixels are relevant to surface geometry. On the other hand, when the specular lobe is narrow, the intensity ratios of most pixels are independent of surface geometry. This suggests that the appropriate determination of threshold T_P should be important for the robust estimation of $\hat{Q}_d$. However, as will be seen in the experiment, a fixed T_P value is sufficient to almost all real scenes.

From Eqs. (4) and (6), the diffuse portion of the reflection $m_d(x)\Lambda_{\max} \approx \hat{Q}_d I_{\text{ran}}$. Hence, the specular component can be computed from the maximum intensity as

$$I^S(x) = \max\{I_{\max}(x) - \hat{Q}_d I_{\text{ran}}, 0\}, \tag{10}$$

where the $\max\{\cdot\}$ operator ensures that the specular component is no less than zero.

With the separated specular component, the diffuse component is computed as

$$\mathbf{I}^D(x) = \mathbf{I}(x) - \mathbf{I}^S(x), \tag{11}$$

where $\mathbf{I}^S(x) = [I^S(x), I^S(x), I^S(x)]^T$. Note that the elements in $\mathbf{I}^S(x)$ are same because the pixel colors have been normalized with respect to the illumination color.

C. Pixel Clustering

When dealing with textured surfaces, Tan and Ikeuchi [12] determined local color discontinuity using simple chromaticity thresholding, which may produce erroneous reflection separation [19]. Instead, we extend the concept of intensity ratio from uniform color surfaces to nonuniform or textured surfaces using pixel clustering.

We adopt the SF image $\mathbf{I}^{\text{SF}}$ as in [18], whose element of channel c, $c \in \{r, g, b\}$, at pixel x is computed as

$$I_c^{\text{SF}}(x) = I_c(x) - I_{\min}(x) + \bar{I}_{\min}, \tag{12}$$

where

$$\bar{I}_{\min} = \frac{\sum_{x=1}^{N} I_{\min}(x)}{N}, \tag{13}$$

where N is number of pixels in the image. We compute the SF chromaticity $\Lambda^{\text{SF}}(x) = [\Lambda_r^{\text{SF}}(x), \Lambda_g^{\text{SF}}(x), \Lambda_b^{\text{SF}}(x)]^T$ as

$$\Lambda^{\text{SF}}(x) = \frac{\mathbf{I}^{\text{SF}}(x)}{I_r^{\text{SF}}(x) + I_g^{\text{SF}}(x) + I_b^{\text{SF}}(x)}. \tag{14}$$

It is found that the SF chromaticity is robust to image noise owing to the inclusion of term $\bar{I}_{\min}$ [18].

As the intensity ratio $Q(x)$ is only related to $\Lambda_{\min}$ and $\Lambda_{\max}$ [see Eqs. (6) and (7)], we construct the pseudo-chromaticity $\Lambda^P(x)$ as

$$\Lambda^P(x) = [\Lambda_{\min}^{\text{SF}}(x), \Lambda_{\max}^{\text{SF}}(x)]^{\text{T}}, \tag{15}$$

where $\Lambda_{\min}^{\text{SF}}(x) = \min\{\Lambda_r^{\text{SF}}(x), \Lambda_g^{\text{SF}}(x), \Lambda_b^{\text{SF}}(x)\}$ and $\Lambda_{\max}^{\text{SF}}(x) = \max\{\Lambda_r^{\text{SF}}(x), \Lambda_g^{\text{SF}}(x), \Lambda_b^{\text{SF}}(x)\}$. We note that two different colors may have the same pseudo-chromaticity. For example, for the red color $(1, 0.3, 0.2)^T$ and green color $(0.2, 1, 0.3)^T$, their pseudo-chromaticity values are both $(0.13, 0.67)^T$. This treatment is appropriate, as the purpose of pixel clustering in this work is to compute intensity ratios, not to separate color regions.

The chromaticity distance between two pixels x and y is defined by using the ℓ_1 norm:

$$d_\Lambda(x, y) = \|\Lambda^P(x) - \Lambda^P(y)\|_1. \tag{16}$$

If the chromaticity distance is less than a threshold T_C, these two pixels are judged to belong to the same cluster; otherwise they are classified into different clusters. The pseudo code for pixel clustering is listed in Algorithm 1.

Algorithm 1 Pixel clustering

Input: Pseudo-chromaticity $\Lambda^P(x)$, threshold T_C
Variables: L: Number of clusters
x_0: First pixel
m_l: Mean pseudo-chromaticity of cluster l
Initialization: $L \leftarrow 1$, label$(x_0) \leftarrow L$, $m_L \leftarrow \Lambda^P(x_0)$
for next unlabeled pixel x_i **do**
  Calculate its distances to all clusters
  $d_l(x_i) = \|\Lambda^P(x_i) - m_l\|_1$, $1 \le l \le L$
  Find the label with minimum distance $d_{\min}(x_i)$
  $l_{\min} = \arg\min_l d_l(x_i)$
  if $d_{\min}(x_i) \le T_C$ **then**
    label$(x_i) \leftarrow l_{\min}$
    Update $m_{l_{\min}}$
  else
    $L \leftarrow L + 1$
    label$(x_i) \leftarrow L$
    $m_L \leftarrow \Lambda^P(x_i)$
  end
end
Output: label(x)

Figure 2 shows the clustering result of a *Fish* image and the intensity ratio map. It is observed that

Fig. 2. Clusters and corresponding intensity ratios of the *Fish* image. (a) Original image and (b) ratio map obtained using thresholds $T_P = 0.2$ and $T_C = 0.2$. This threshold setting results in four clusters, with estimated intensity ratios $\hat{Q}_d = 1.93$, 1.37, 1.26, and 1.22. The ratio map is enhanced for visualization.

the computed cluster number is less than the region number of the original image. As mentioned, this is partially due to the ordering nature of the pseudo-chromaticity space Λ^P; actually opponent colors may have similar pseudo-chromaticity values. In addition, a relatively large chromaticity threshold T_C will also result in a decreased cluster number.

D. Outline of the Algorithm

Based on the above discussion, we summarize the procedure of specular highlight removal as follows:

1. Compute the pseudo-chromaticity image;
2. Classify pixels into appropriate clusters according to the specified chromaticity threshold T_C;
3. Determine the intensity ratio of each cluster by using the specified percentile threshold T_P;
4. Separate diffuse and specular reflection components.

3. Experiment

We evaluated the proposed and existing methods [12,18,19] using qualitative visual perception and the quantitative peak signal-to-noise ratio (PSNR). We note that the human visual system is insensitive to color changes in large areas, but sensitive to color changes at edges. Instead, the PSNR measures image difference on a pixel-wise basis and treats all pixels equally. Hence, it can be considered that the quantitative and qualitative evaluations are complementary in image similarity assessment. When the visual appearances of the separated diffuse images obtained by two competitive methods are close, we regard PSNR as an important quantitative measure.

In addition to the global PSNR computed on the whole image, in this paper we also employ regional PSNR computed in highlight areas. These two PSNR values can, respectively, reflect the global and regional reliability of the highlight removal methods.

We captured images of four real scenes, namely, *Masks*, *Cup*, *Fruit*, and *Animals* (see Figs. 4, 5, 6, and 7), for quantitative analysis. The scenes were illuminated by using white light-emitting diodes (LEDs), and the ground truth diffuse images were acquired by placing polarization filters in front of the camera and the LEDs. These images appear dark because of the well-controlled experimental condition. With the ground truths, we analyzed the threshold effect of the proposed method and evaluated the highlight removal accuracy in terms of PSNR. We also conducted experiments on scenes illuminated by more light sources (fluorescent lamps and LEDs) for qualitative analysis. These images (see Figs. 8–10) contain more highlight regions and appear bright. Note that these images are nonlinearly enhanced in this paper for visualization purposes.

In the experiments, the illumination chromaticity was acquired by imaging a white diffuse board, and the captured images were normalized with respect to the illumination color, as mentioned in Section 2. The camera exposure time is controlled such that the highlight pixels in these images were not saturated. In the case of color saturation, the images could probably be recovered by using channel correlations [25], but this is beyond of the scope of this work.

The proposed method was implemented in C++ on a personal computer with 2.66 GHz CPU and 2 GB RAM. The sources codes of Tan's method [12] and Yang's method [19] were downloaded from the authors' websites [26,27]. They were both written in C++. We compared the computational efficiency of the proposed method with Yang's method, which is, to our knowledge, the fastest up to date.

A. Effect of Thresholds

It is known that parameters usually affect the performance of an algorithm. Figure 3 shows the effect of chromaticity threshold T_C and percentile threshold T_P in terms of global PSNR. It is observed that, for three images (*Cups*, *Fruit*, and *Animals*), the changes of PSNR values are more distinct along the T_P direction than along the T_C direction, indicating that

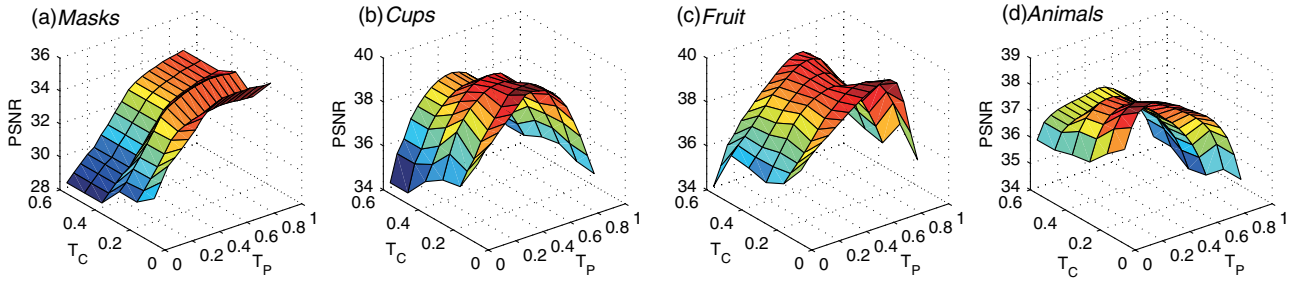

Fig. 3. Distributions of global PSNR values with respect to the chromaticity threshold T_C and percentile threshold T_P for the images.

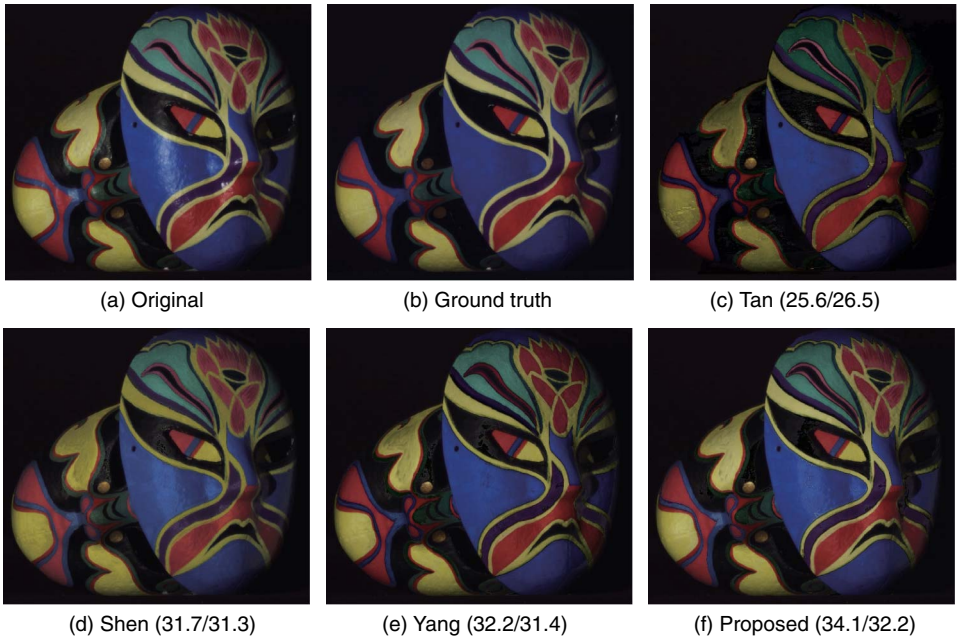

Fig. 4. Separated diffuse reflection components of the *Masks* image using different methods. The global and regional PSNR values are, respectively, shown in the parenthesis.

the percentile threshold is more influential to the algorithm performance. The *Masks* image exhibits a similar distribution, although not quite obvious.

Figure 3 implies that scene analysis is necessary to achieve optimal highlight removal for individual images. However, by fixing the thresholds $T_C = 0.3$ and $T_P = 0.5$, the proposed method can produce quite satisfactory results on all these images, in terms of both PSNR and visual appearance. As will be seen in the following, these fixed thresholds are also suitable for other images. Therefore, we consider that this treatment of thresholds is appropriate for practical applications.

B. Results

Figure 4 illustrates the separated diffuse reflections of the *Masks* image that contains heavy textures using different methods. It is observed that Tan's method [12] removes too much specular reflection and thus produces quite low PSNR values. The diffuse images by Shen's method [18] and Yang's method [19] are relatively better. In comparison, the proposed method produces faithful appearance and the highest PSNR values. Figure 5 shows the separated diffuse reflections of two cup surfaces that contain girl and monkey drawings. In Tan's result [Fig. 5(c)], The girl's face area is separated into

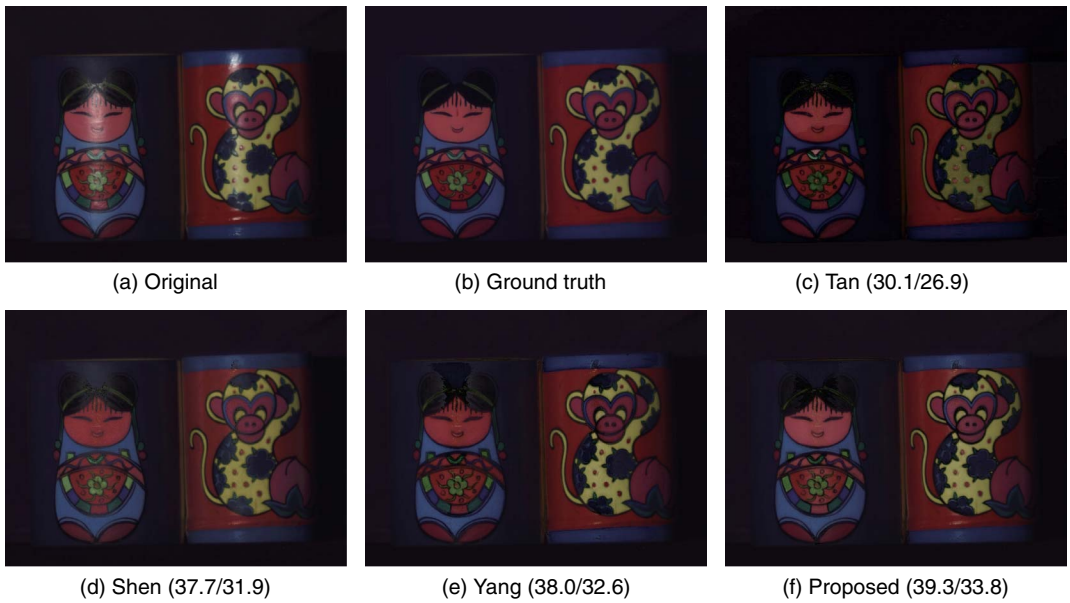

Fig. 5. Separated diffuse reflection components of the *Cups* image using different methods. The global and regional PSNR values are, respectively, shown in the parenthesis.

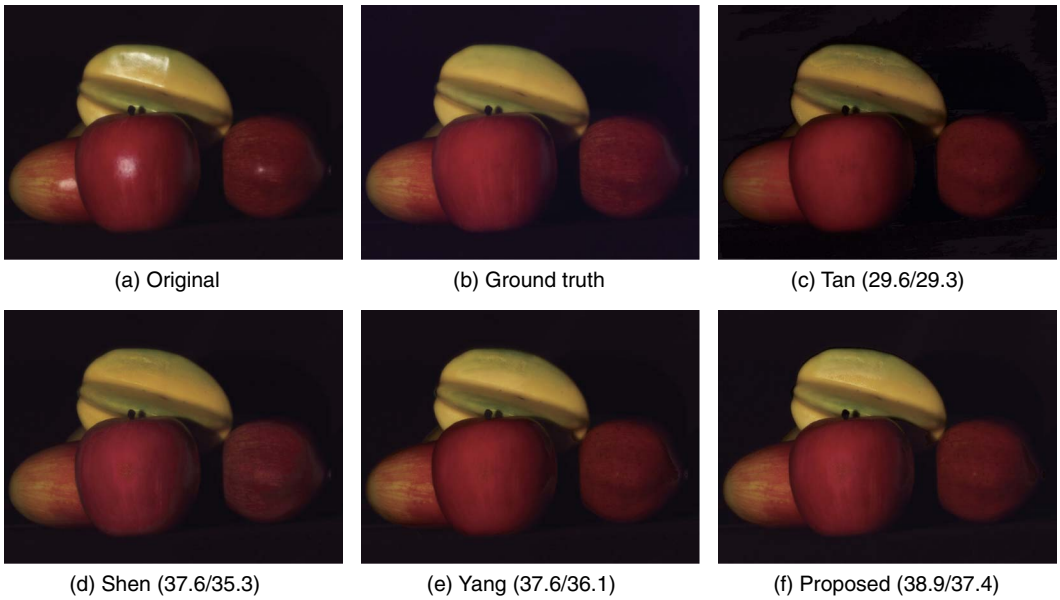

(a) Original (b) Ground truth (c) Tan (29.6/29.3)

(d) Shen (37.6/35.3) (e) Yang (37.6/36.1) (f) Proposed (38.9/37.4)

Fig. 6. Separated diffuse reflection components of the *Fruit* image using different methods. The global and regional PSNR values are, respectively, shown in the parenthesis.

two regions, probably due to the method's unreliability in determining color boundaries. The diffuse component obtained by the proposed method, although not perfect, is quantitatively the most accurate one. Figure 6 shows the separation results on the *Fruit* image, which has various shapes of highlight on individual surfaces. Again, the proposed method produces satisfactory separation result and achieves the highest PSNR values. In Fig. 7, the highlight on the rabbits' ears is quite difficult to remove, and Shen's method produces visually good diffuse component in these areas. In terms of global PSNR, Yang's method and the proposed method perform similarly, but in terms of regional PSNR, Yang's method performs better.

It is of interest to evaluate the performances of highlight removal methods with respect to image noise. We simulated corrupted images by using additive Gaussian noise with zero mean and standard deviation (noise level) $\sigma = 3$ and 6. The experimental results are shown in Table 1, where $\sigma = 0$ means without image noise. As expected, the PSNR values of all methods decrease when the noise level σ changes from 0 to 6. The proposed method results in

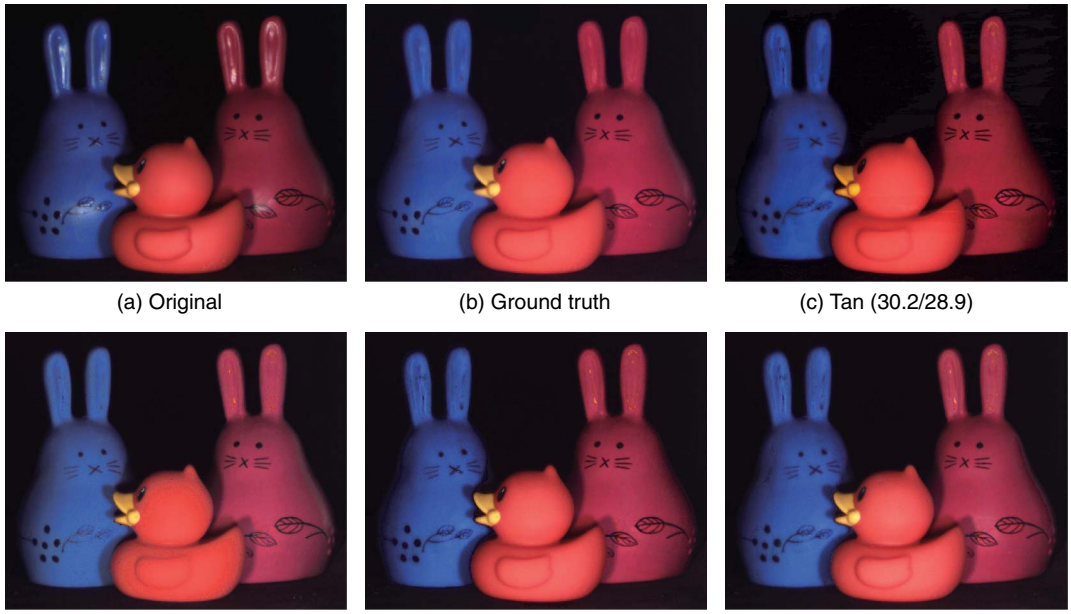

(a) Original (b) Ground truth (c) Tan (30.2/28.9)

(d) Shen (34.6/31.9) (e) Yang (37.2/33.9) (f) Proposed (37.3/32.6)

Fig. 7. Separated diffuse reflection components of the *Animals* image using different methods. The global and regional PSNR values are, respectively, shown in the parenthesis.

Table 1. Global and Regional PSNR Values of Reflection Separation Methods When Images are Corrupted by Additive Gaussian Noise with Various Noise Levels (σ)[a]

		Global PSNR				Regional PSNR			
Image	σ	Tan	Shen	Yang	Proposed	Tan	Shen	Yang	Proposed
	0	25.6	31.7	32.2	**34.1**	26.5	31.3	31.4	**32.2**
Masks	3	25.6	30.5	29.8	**32.5**	26.4	30.6	29.6	**31.4**
	6	25.6	28.8	27.5	**29.9**	26.1	28.9	27.5	**29.2**
	0	30.1	37.7	38.0	**39.3**	26.9	31.9	32.6	**33.8**
Cups	3	30.0	34.4	34.1	**35.5**	26.6	29.6	30.3	**31.6**
	6	29.3	31.4	30.0	**31.8**	25.8	28.0	26.6	**28.8**
	0	29.6	37.6	37.6	**38.9**	29.3	35.3	36.1	**37.4**
Fruit	3	29.2	34.0	34.0	**35.5**	26.6	32.4	31.9	**33.9**
	6	28.9	30.7	30.1	**31.8**	26.7	29.2	27.6	**30.1**
	0	30.2	34.6	37.2	**37.3**	28.9	31.9	**33.9**	32.6
Animals	3	27.4	32.6	34.4	**35.2**	26.0	31.9	32.3	**32.4**
	6	26.5	30.8	30.4	**31.6**	25.4	**30.2**	28.5	29.0

[a]The highest global and regional PSNR values are in bold.

highest global PSNR values in all cases and highest regional PSNR values in most cases, except for the *Animal* images when $\sigma = 0$ and 6. This validates the superiority of the proposed method over its competitors under the quantitative measure.

We conducted highlight removal on three other scenes, namely *Watermelon*, *Rabbit*, and *Wood*, which are illuminated by two fluorescent lamps and two LEDs. As ground truths are not available, we compare the visual appearances of the resultant diffuse images by different methods. In Fig. 8, Tan's method produces a quite dark diffuse component, and Yang's method fails to remove the highlight spots on the watermelon surface. The proposed method successfully removes the highlights on the cat and watermelon surfaces, and visually performs better than all other methods. In Fig. 9, Tan's method produces erroneous results on the rabbit's body. The highlight spots on the rabbit's ears and body are not completely removed by Shen's and Yang's methods. In comparison, the resultant diffuse image obtained by the proposed method is satisfactory in these areas. However, the inset in Fig. 9(e) indicates that the proposed method produces an artificial dark band along the boundary between the rabbit's head and the background. This is because in this boundary area the light entering into the camera is quite low and the pixel colors are less saturated or nearly achromatic. Consequently, the intensity ratios and pseudo-chromaticity values in this area are not reliable. In Fig. 10, Tan's method fails, and Shen's method cannot remove the highlight stripe on the three-color cylinder completely. The diffuse image produced by the proposed method is close to that by Yang's method, in which the highlight stripe is successfully removed. However, the masked white surface in Fig. 10(e) is judged as specular highlight because of its neutral chromaticity, and it becomes darker in the separated diffuse component. Yang's

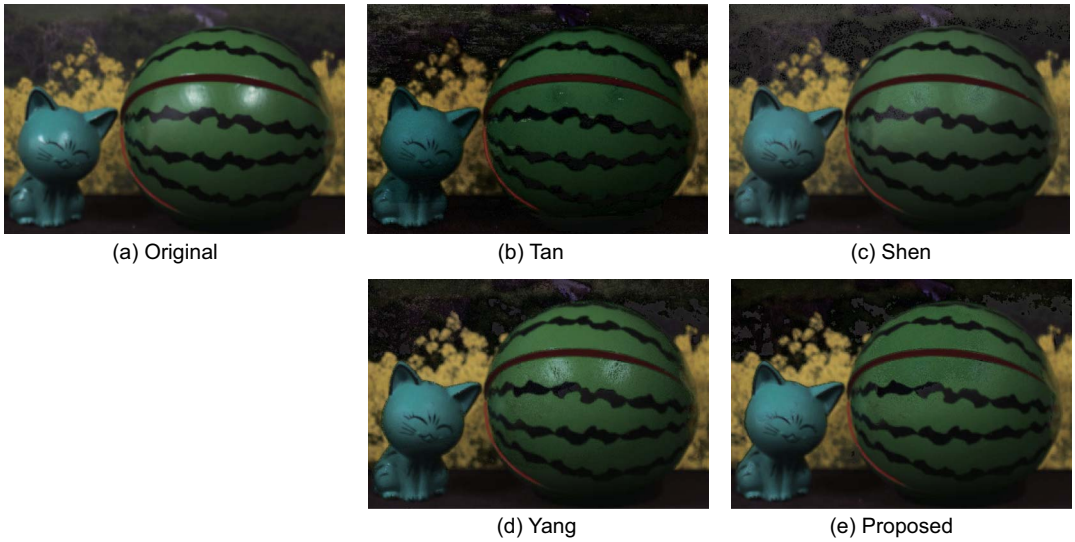

Fig. 8. Separated diffuse reflection components of the *Watermelon* image using different methods.

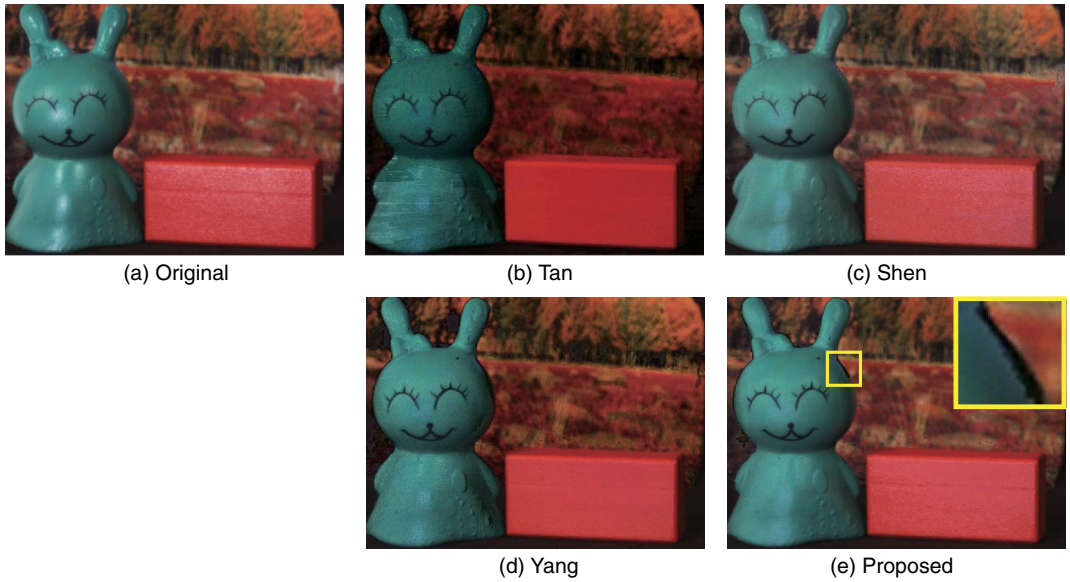

Fig. 9. Separated diffuse reflection components of the *Rabbit* image using different methods. The inset in (e) indicates a limitation of the proposed method in a dark boundary area.

method also fails on this white surface, and Shen's method performs relatively better.

We also evaluated the proposed method on images with complex surfaces, namely *Fish* and *Toys*, which were used in previous work [12]. The results are shown in Figs. 11 and 12. It can be seen that the diffuse reflections obtained by the proposed method are visually satisfactory and competitive to those obtained by other methods.

In addition to the accuracy of reflection separation, the computational efficiency is also essential for practical applications. The proposed method runs in a pixel-wise manner, involving pseudochromaticity computation, pixel clustering, quick data sorting, and reflection component computation. As only arithmetic and comparing operations are needed in these computations, the implementation of the proposed method is very simple and efficient. In comparison, the implementation of Yang's method is much complicated, requiring the interaction between neighboring pixels in bilateral filtering [27]. To speed up bilateral filtering, the authors use recursive approximation of a Gaussian filter, image downsampling, and range function quantization. Table 2 lists the computational times (in seconds) of the proposed method and Yang's method on the mentioned personal computer. Thanks to the simple computation, the proposed method runs 4× faster than Yang's method on average.

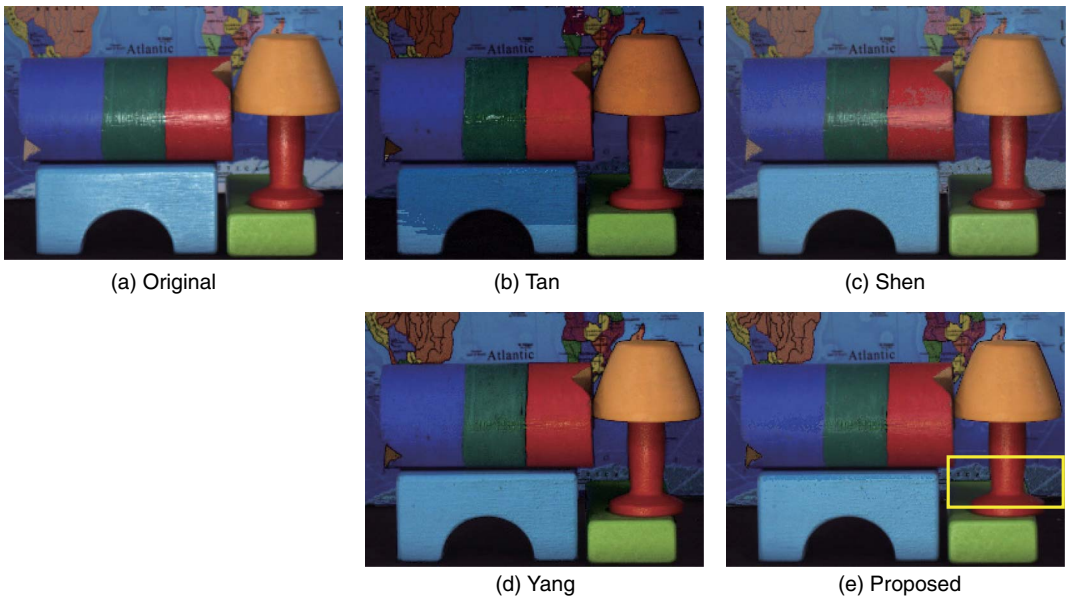

Fig. 10. Separated diffuse reflection components of the *Wood* image using different methods. The masked area in (e) indicates a limitation of the proposed method on a white surface.

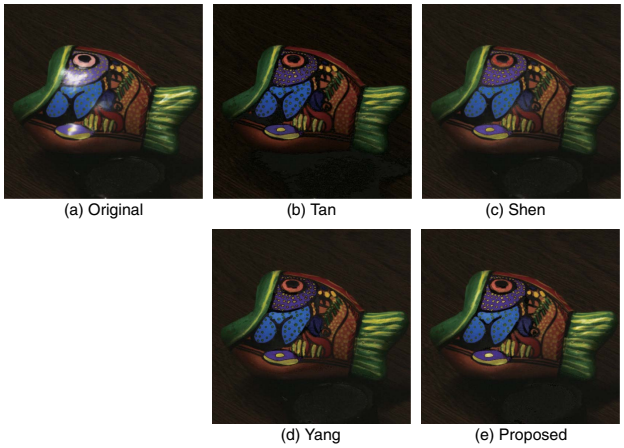

Fig. 11. Separated diffuse reflection components of the *Fish* image using different methods.

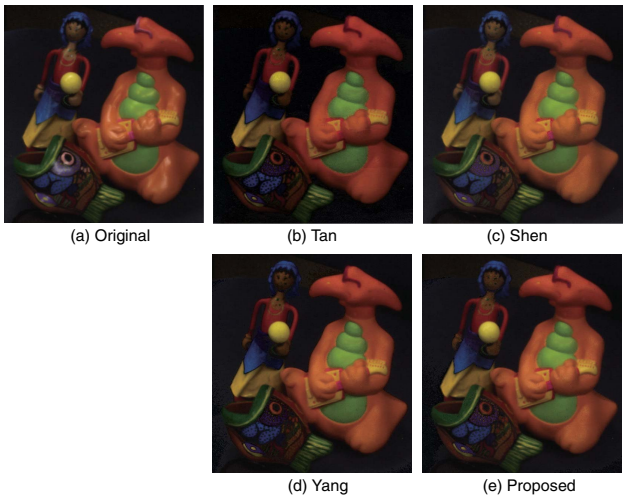

Fig. 12. Separated diffuse reflection components of the *Toys* image using different methods.

Table 2. Computational Time (in seconds) of Yang's Method [19] and the Proposed Method on a Personal Computer

Image	Size (pixels)	Yang	Proposed	Speedup
Masks	500 × 450	0.203	0.037	5.5
Fruit	640 × 480	0.172	0.051	3.4
Cups	640 × 480	0.201	0.042	4.8
Animals	396 × 321	0.094	0.023	4.1
Watermelon	379 × 255	0.063	0.015	4.2
Rabbit	377 × 279	0.156	0.016	9.8
Wood	271 × 203	0.078	0.015	5.2
Fish	490 × 480	0.109	0.022	5.0
Toys	353 × 387	0.172	0.023	7.5

4. Conclusions

This paper has proposed a new real-time method for the separation of diffuse and specular reflection components in a single image. To deal with multicolored and textured surfaces, pixels are classified into different clusters in a pseudo-chromaticity space. The specular reflection component of each pixel is computed based on the corresponding intensity ratio, which is independent of surface geometry. Unlike existing techniques, the proposed method is implemented on the individual pixel basis, without employing an iterative framework and identifying specular pixels. Experimental results validate that, in comparison with the state-of-the-art techniques, the proposed method performs better in terms of both highlight removal accuracy and computational efficiency. The limitations of the proposed method are that it cannot produce satisfactory results on dark and achromatic surfaces. Our future work is to resolve these limitations and further improve the computational speed such that the method can be applied in general-purpose applications.

This work was supported by the National Basic Research Program of China under grant 2009CB320801 and the National Natural Science Foundation of China under grant nos. 60778050 and 61271339.

References

1. T. Gevers and H. Stokman, "Classifying color edges in video into shadow-geometry, highlight, or material transitions," IEEE Trans. Multimedia **5**, 237–243 (2003).
2. R. T. Tan, K. Nishino, and K. Ikeuchi, "Color constancy through inverse-intensity chromaticity space," J. Opt. Soc. Am. A **21**, 321–334 (2004).
3. J. Toro and B. Funt, "A multilinear constraint on dichromatic planes for illumination estimation," IEEE Trans. Image Process. **16**, 92–97 (2007).
4. Q. Yang, S. Wang, N. Ahuja, and R. Yang, "A uniform framework for estimating illumination chromaticity, correspondence and specular reflection," IEEE Trans. Image Process. **20**, 53–63 (2011).
5. S. P. Mallick, T. E. Zickler, D. J. Kriegman, and P. N. Belhumeur, "Beyond Lambert: reconstructing specular surfaces using color," in *IEEE Computer Society Conference on Computer Vision and Pattern Recognition, 2005. CVPR 2005* (IEEE Computer Society, 2005), Vol. **2**, pp. 619–626.
6. D. Miyazaki, K. Hara, and K. Ikeuchi, "Median photometric stereo as applied to the Segonko tumulus," Int. J. Comput. Vis. **86**, 229–242 (2010).
7. H. C. Lee, D. J. Breneman, and C. O. Schulte, "Modeling light reflection for computer color vision," IEEE Trans. Pattern Anal. Mach. Intell. **12**, 402–409 (1990).
8. A. Artusi, F. Banterle, and D. Chetverikov, "A survey of specularity removal methods," Comput. Graph. Forum **30**, 2208–2230 (2011).
9. G. J. Klinker, S. A. Shafer, and T. Kanade, "The measurement of highlights in color images," Int. J. Comput. Vis. **2**, 7–32 (1988).
10. Y. Sato and K. Ikeuchi, "Temporal-color space analysis of reflection," J. Opt. Soc. Am. A **11**, 2990–3002 (1994).
11. R. T. Tan, K. Nishino, and K. Ikeuchi, "Separating reflection components based on chromaticity and noise analysis," IEEE Trans. Pattern Anal. Mach. Intell. **26**, 1373–1379 (2004).
12. R. T. Tan and K. Ikeuchi, "Separating reflection components of textured surfaces using a single image," IEEE Trans. Pattern Anal. Mach. Intell. **27**, 178–193 (2005).
13. R. T. Tan and K. Ikeuchi, "Reflection components decomposition of texured surfaces using linear basis functions," in *IEEE Computer Society Conference on Computer Vision and Pattern Recognition, 2005. CVPR 2005* (IEEE Computer Society, 2005), Vol. **1**, pp. 125–131.

14. S. K. Nayar, X. S. Fang, and T. Boult, "Separation of reflection components using color and polarization," Int. J. Comput. Vis. **21**, 163–186 (1997).
15. S. Lin, Y. Li, S. B. Kang, X. Tong, and H.-Y. Shum, "Diffuse-specular separation and depth recovery from image sequences," in *Computer Vision—ECCV 2002* (Springer, 2002), pp. 210–224.
16. P. Tan, S. Lin, L. Quan, and H. Y. Shum, "Highlight removal by illumination-constrained inpainting," in *Ninth IEEE International Conference on Computer Vision* (IEEE, 2003), Vol. **1**, pp. 164–169.
17. S. P. Mallick, T. E. Zickler, P. N. Belhumeur, and D. J. Kriegman, "Specularity removal in images and videos: a PDE approach," in *Computer Vision—ECCV 2006* (Springer, 2006), Vol. **1**, pp. 550–563.
18. H. L. Shen, H. G. Zhang, S. J. Shao, and J. H. Xin, "Chromaticity-based separation of reflection components in a single image," Pattern Recogn. **41**, 2461–2469 (2008).
19. Q. Yang, S. Wang, and N. Ahuja, "Real-time specular highlight removal using bilateral filtering," in *Computer Vision–ECCV 2010* (Springer, 2010), pp. 87–100.
20. H. L. Shen and Q. Y. Cai, "Simple and efficient method for specularity removal in an image," Appl. Opt. **48**, 2711–2719 (2009).
21. S. A. Shafer, "Using color to separate reflection components," Color Res. Appl. **10**, 210–218 (1985).
22. S. Barsky and M. Petrou, "The 4-source photometric stereo technique for three-dimensional surfaces in the presence of highlights and shadows," IEEE Trans. Pattern Anal. Mach. Intell. **25**, 1239–1252 (2003).
23. J. van de Weijer and T. Gevers, "Edge-based color constancy," IEEE Trans. Image Process. **16**, 2207–2214 (2007).
24. K. J. Yoon and I. S. Kweon, "Voting-based separation of diffuse and specular pixels," Electron. Lett. **40**, 1260–1261 (2004).
25. D. Xu, C. Doutre, and P. Nasiopoulos, "Correction of clipped pixels in color images," IEEE Trans. Vis. Comput. Graph. **17**, 333–344 (2011).
26. R. T. Tan, "Specular highlight removal from a single image," http://people.cs.uu.nl/robby/code.html.
27. Q. Yang, "Real-time specular highlight removal using bilateral filtering," http://www.cs.cityu.edu.hk/~qiyang/.